Mapping Nanoscale Electrochemistry of Individual Single-Walled Carbon Nanotubes

ARTICLE *in* NANO LETTERS · NOVEMBER 2013

Impact Factor: 13.59 · DOI: 10.1021/nl403752e · Source: PubMed

NANO LETTERS

Letter

pubs.acs.org/NanoLett

Mapping Nanoscale Electrochemistry of Individual Single-Walled Carbon Nanotubes

Aleix G. Güell,[†] Katherine E. Meadows,[†,‡] Petr V. Dudin,[†] Neil Ebejer,[†] Julie V. Macpherson,[†] and Patrick R. Unwin*[,†]

[†]Department of Chemistry and [‡]Molecular Organisation and Assembly in Cells Doctoral Training Centre, University of Warwick, Coventry, CV4 7AL, United Kingdom

Supporting Information

ABSTRACT: We introduce a multiprobe platform for the investigation of single-walled carbon nanotubes (SWNTs) that allows the electrochemical response of an individual SWNT to be mapped at high spatial resolution and correlated directly with the intrinsic electronic and structural properties. With this approach, we develop a detailed picture of the factors controlling electrochemistry at SWNTs and propose a definitive model that has major implications for future architectures of SWNT electrode devices.

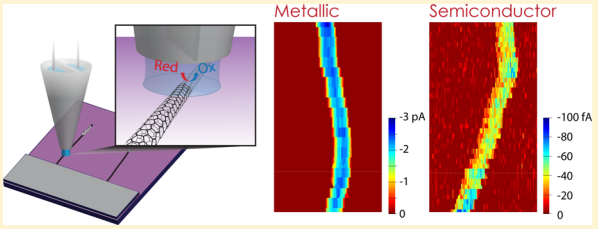

KEYWORDS: *Functional imaging, heterogeneous electron transfer, carbon materials, scanning electrochemical cell microscopy*

Carbon nanotubes have considerable potential as building blocks in the creation of new types of electrochemical interfaces and devices for energy storage and utilization,[1] electrocatalysis,[2] and electrochemical sensing.[3] Yet, the rational design of carbon nanotube electrodes has been hampered by a lack of understanding of structural controls on electrochemical activity. Hitherto, models for electrochemical processes at carbon nanotubes have been dominated by information derived from large ensembles.[4,5] Although such measurements are much simpler than investigations of individual carbon nanotubes,[6−9] they have missed important features that may impact the electrochemistry significantly such as the wide range of electronic properties exhibited by single-walled carbon nanotubes (SWNTs)[10−13] from semiconducting to conducting. In fact, macroscopic measurements have led to commonly used microscopic models for electrochemistry at SWNTs[4] that are at odds with the few microscopic measurements available.[6−9] With the platform described herein, we are able to investigate the interplay of multiple related properties, structure, electronic characteristics, and nanoscale electroactivity, for the first time, allowing us to identify the key factors controlling electrochemistry at SWNTs.

We make use of pristine, as-grown millimeter-long flow-aligned SWNTs grown via catalytic chemical vapor deposition (cCVD) onto an insulating Si/SiO_2 substrate (Figure 1a) in an arrangement where the catalyst is deposited on one side of the substrate from where the SWNT grows.[14] A macroscopic electrical contact was applied at this terminus by thermal evaporation of Pd[15] using a shadow mask, thereby avoiding lithographic procedures that could contaminate the SWNTs.[6,8] To enable ready visualization of the aligned SWNTs by optical microscopy,[16] the SWNTs were marked at the other end by means of silver electrodeposition using a moveable micropipet[8] (all experimental details can be found in the Supporting Information). This approach delineated a portion of an individual pristine SWNT a few hundred micrometers long that could be investigated by a range of complementary high-resolution techniques (Figure 1b).

Scanning electrochemical cell microscopy[7,17−22] (SECCM) was used to investigate the electrochemical activity of individual SWNTs at the nanoscale; Figure 1b. Dual channel (theta) pipets with tip openings of approximately 400−500 nm across were fabricated by a laser puller procedure and characterized fully, defining a mobile meniscus electrochemical cell (see Supporting Information Section S2 for details). Briefly, the approach and scan of the meniscus across the sample was carried out with a highly controllable piezoelectric positioning instrument. Chloridized silver wires inserted into each barrel of the pipet, filled with the solution of interest (redox-active species and supporting electrolyte) acted as quasi-reference counter electrodes (QRCEs). A bias V_2 applied between the QRCEs generated a conductance current (I_2) between the two barrels to aid positioning of the thin liquid meniscus (see Supporting Information Section S2). To drive electrochemical reactions at the SWNT, a bias V_1 was applied, so that the effective applied potential[17,21] to the SWNT was $V_{appl} = -V_1 - V_2/2$ with respect to the QRCE.[7,17−22] Thus, when the SWNT was in contact with the meniscus, an amperometric current (I_{EC}) was detected. This meniscus footprint size ensured that only one or zero defects would typically be accessed with the meniscus centered over an SWNT, considering the highest reported defect ratio for this type of CVD-grown SWNT.[11] Morever, the spatial resolution increased to the nanometer-level

Received: October 8, 2013
Revised: November 14, 2013

   dx.doi.org/10.1021/nl403752e | *Nano Lett.* XXXX, XXX, XXX−XXX

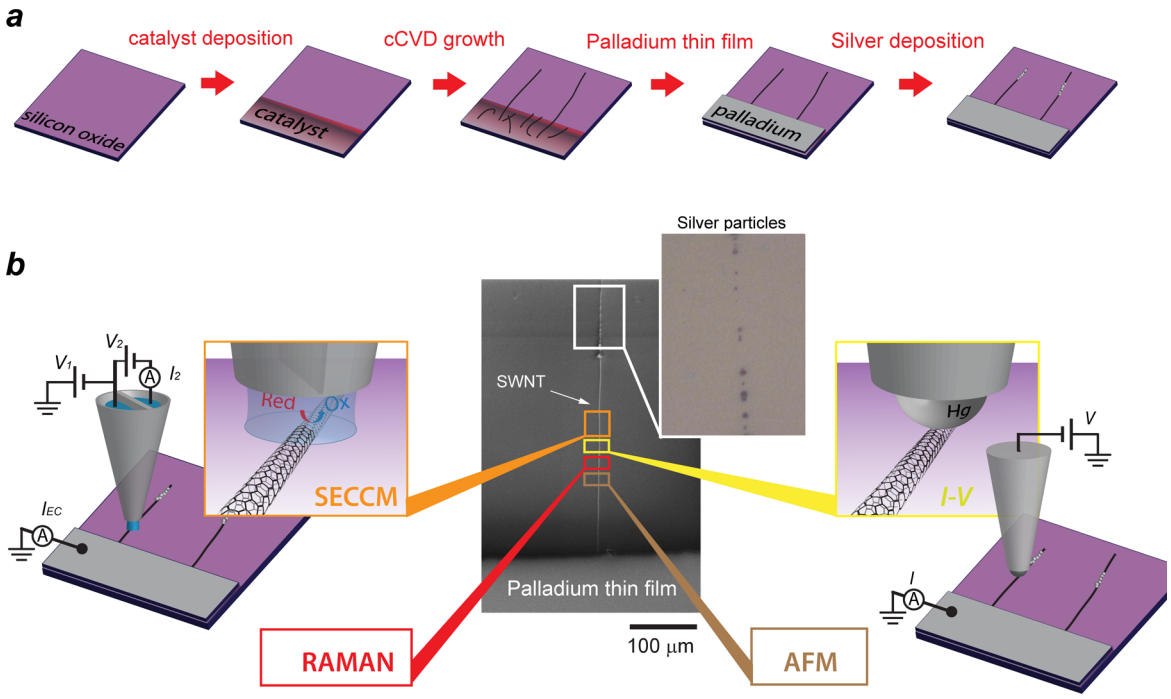

Figure 1. (a) Sequence of steps for sample fabrication. Flow-aligned SWNTs were grown on a silicon/silicon oxide wafer by cCVD, depositing the iron catalyst only on one portion of the sample, so that SWNTs grew across the surface extending into the region that was catalyst free. A macroscopic electrical contact to the SWNTs was achieved by thermal evaporation of a palladium thin film in the region of the catalyst layer. One end of each nanotube was decorated by Ag particles via electrodeposition to make their location visible by optical microscopy. (b) SEM image of a final device, showing an as-grown SWNT, delineated by a macroscopic Pd thin film contact at one end and silver decoration at the other (inset optical microscopy image of an ensemble of silver particles decorating an SWNT). Schematic of the experimental setup for SECCM imaging (left-hand side) and for mercury drop contact conductance measurements (right-hand side). Schematics are not to scale. Raman spectroscopy and atomic force microscopy (not shown) were further deployed to characterize individual SWNT devices.

when the meniscus was scanned over an SWNT while tracking the electrochemical response profile (vide infra).

Two completely different nanotube configurations are considered herein to illustrate the versatility and the key information attainable with the platform. These were two metallic SWNTs bundled together (labeled as "metallic" in the figures that follow) and an isolated individual semiconducting SWNT. These were identified by $I-V$ curves[23,24] and micro-Raman spectroscopy, as described in detail in Supporting Information. Conductance current (I) voltage (V) traces were recorded by establishing a second moveable electrical contact[25] to the other end of the SWNT using a 25 μm diameter Hg-hemisphere droplet electrodeposited on a Pt microdisc (Figure 1b and Supporting Information). The probe was brought into contact with the sample by means of a micropositioner, and once contact was made between an SWNT and the Hg-UME probe, the bias, V, was swept to obtain conductance $I-V$ traces, revealing the electronic nature of each individual nanotube.

A series of electrochemical current maps were obtained for two well-known and widely studied outer-sphere redox processes, the one-electron oxidation of ferrocenylmethyl-(trimethylammonium) ($FcTMA^+$) and the one-electron reduction of ruthenium(III) hexamine ($Ru(NH_3)_6^{3+}$). For the oxidation of $FcTMA^+$ at the metallic and semiconducting SWNT devices, at different working electrode potentials (Figure 2a) the immediate and striking observation is that both devices show essentially uniform electrochemical activity along the entire length of SWNT, demonstrating that pristine SWNT sidewalls, as the only part accessed, are highly active toward heterogeneous electron transfer (HET), in contrast to the widely assumed model that pictures the SWNT sidewall as electrochemically inert, even for simple redox couples.[4] The narrow distribution of peak current values, at each potential for trace and retrace scans, confirms the uniformity of the electrochemical (EC) activity during a scan along an SWNT (Figure 2b). This behavior was characteristic of >10 devices investigated (~50 μm length each).

The SECCM response was analyzed quantitatively using finite element method (FEM) modeling,[21] considering a standard Butler–Volmer model for electron transfer (ET)[26] (see Supporting Information). We assume a transfer coefficient $\alpha = 0.5$, which is reasonable for fast outer sphere redox processes and applicable to both metallic and semiconductor SWNTs, since in the potential range of $FcTMA^+$ oxidation the p-type semiconductor SWNT will be in the charge accumulation state and is thus metal-like.[6,26,27] Comparison of the entire data set of redox peak currents (i.e. with the meniscus centered over a portion of an SWNT) at each potential to simulations for a wide range of standard rate constant values, k_0 (from 1 to 50 cm s^{-1}), yielded $k_0 = 7 \pm 2$ cm s^{-1} for the metallic configuration, and $k_0 = 4 \pm 2$ cm s^{-1} for the semiconducting SWNT (Figure 2b). Note that the mass transport-limited current (at $V_{appl} = 0.5$ V) was similar for the metallic configuration and semiconducting SWNT, suggesting that they have a similar effective area and could be modeled with the same effective geometry (Supporting Information). The kinetic analysis was also performed separately for potentials where the current could be measured accurately ($I_{EC} > 600$ fA) but away from the diffusion-limit ($V_{appl} = 0.25$, 0.3, and 0.35 V) (Supporting Information Section S3). The k_0

dx.doi.org/10.1021/nl403752e | Nano Lett. XXXX, XXX, XXX–XXX

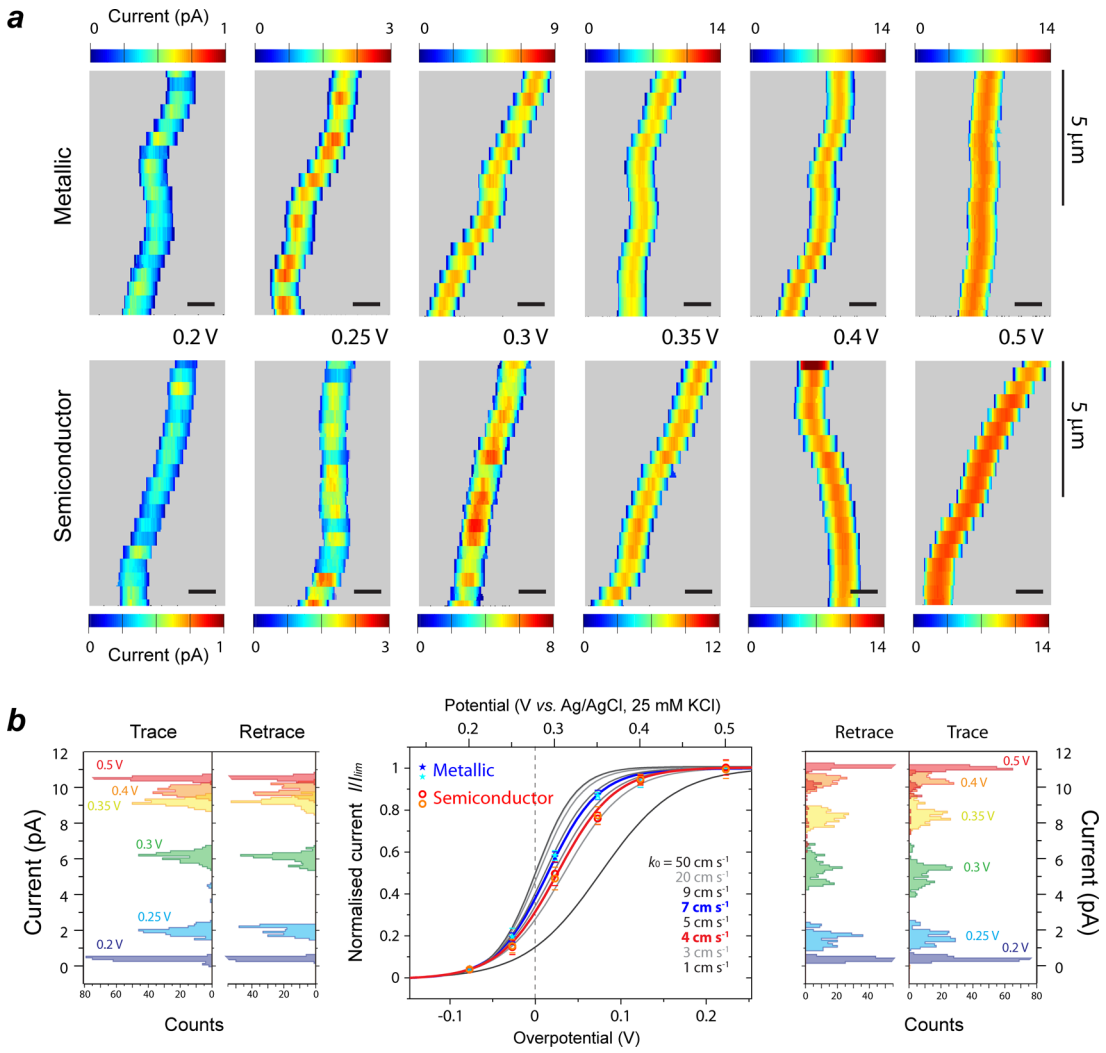

Figure 2. (a) Set of SECCM surface current maps for the oxidation of 2 mM ferrocenylmethyl(trimethylammonium) in 25 mM KCl and phosphate buffer (pH = 7.2) at two individual SWNTs (metallic and semiconductor) at different driving potentials (from V_{appl} = 0.2−0.5 V vs Ag/AgCl, 25 mM KCl). Scale bar on the *x*-axis (perpendicular to the SWNT) is 500 nm. Color values are assigned when the signal is detectable at 3 times above the background current (10 fA), otherwise the current is assigned to the background (gray). (b) The peak currents from each line in each map plotted as histograms for both trace and retrace scans for all the potentials employed. The average value is plotted with respect to the applied potential and overpotential, together with the simulated steady-state linear sweep voltammograms with different standard rate constants, k_0. Error bars indicate 1 standard deviation. Histograms are for the metallic SWNT configuration on the left hand side and semiconductor SWNT on the right hand side.

values extracted at each potential were consistent with the overall profiles in Figure 2b and comparable to those reported for standard pure metal electrodes, such as Pt[28,29] as well as SWNTs,[6,7] indicating that pristine SWNTs can readily be used as electrodes where outer-sphere redox species are deployed and that no modification of the surface to produce defect features is needed to promote electrochemistry at the sidewalls.[4,5]

The intrinsic electrochemical activity of the SWNT sidewall was analyzed with nanoscale spatial resolution by considering SECCM scan profiles, since the redox current was collected at 6 nm intervals along each line scanned by the pipet meniscus. As the meniscus moves from the Si/SiO_2 substrate to the SWNT, the electrochemical current gradually rises as an increasing length of the SWNT is exposed to the solution, reaching a peak current value when the center of the pipet (meniscus) is directly over the SWNT (data analyzed above), and then falling as the pipet moves on. This analysis was, furthermore, carried out as a function of potential on an individual SWNT, by changing the electrochemical potential for different scan profiles (Figure 3a). The experimental line profile (Figure 3b) was compared to theory using the known geometry of the pipet tip (Supporting Information Section S2) and footprint of the meniscus, revealed from the profile width. The excellent agreement between the experimental data points along the profile (trace and retrace scans) with the simulated curve (assumed a uniformly active SWNT and the previously determined k_0 value for the "metallic" SWNT configuration) at the different potentials studied is conclusive proof of the highly uniform activity of SWNTs and rules out the possibility that the response is governed solely by specific defects, which are at a much lower density (wider spacing) than the 6 nm resolution delivered by SECCM line profile measurements (vide supra).

To explore differences in electrochemical behavior between metallic and semiconducting SWNT devices, we investigated the reduction of $Ru(NH_3)_6^{3+}$. The presence of a large Schottky barrier for electron injection in metal-semiconductor con-

dx.doi.org/10.1021/nl403752e | *Nano Lett.* XXXX, XXX, XXX−XXX

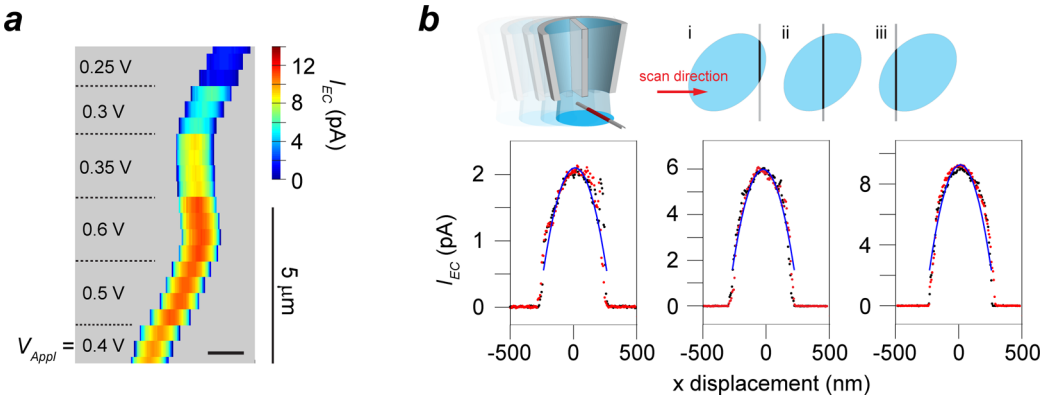

Figure 3. (a) SECCM electrochemical map along an individual metallic SWNT for the oxidation of 2 mM ferrocenylmethyl(trimethylammonium) in 25 mM KCl and phosphate buffer (pH = 7.2) at a set of distinct applied potentials. Scale bar on the *x*-axis is 500 nm. Color values are assigned when the signal is detectable at 3 times above the background current (10 fA), otherwise the current is assigned to the background (gray). (b) Schematic of the SECCM probe meniscus scanning across an SWNT, illustrating how at three different positions (i, ii, and iii) the SWNT length accessed is different. Comparison between experimental scan profiles (trace red dots, retrace black dots) extracted from the EC map in (a) at different potentials (from left to right, V_{appl} = 0.25 V, V_{appl} = 0.3 V, and V_{appl} = 0.35 V) and simulated scan profiles for k_0 = 7 cm s^{-1} (blue line). To aid comparison, forward and reverse scan profiles were centered (*x*-displacement 0 nm) at the peak current position.

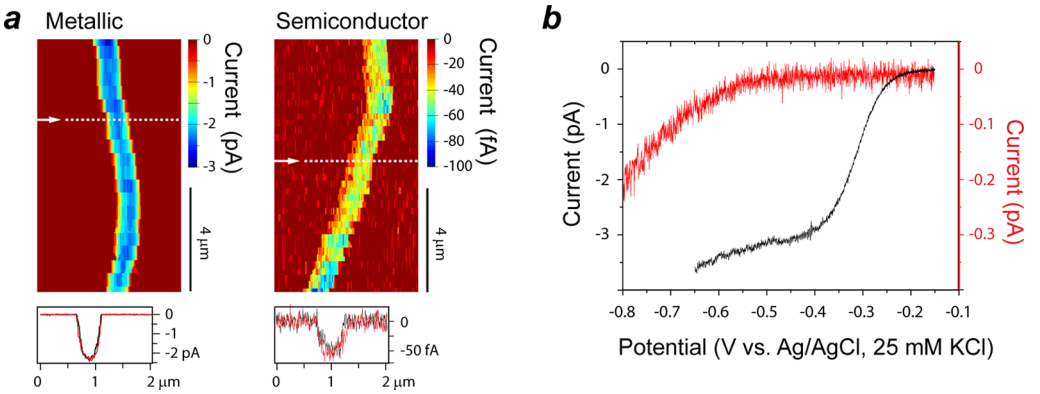

Figure 4. (a) SECCM electrochemical (EC) current maps for the reduction of 0.5 mM $Ru(NH_3)_6^{3+}$ (25 mM KCl and phosphate buffer, pH = 7.2) at metallic and semiconducting SWNT devices. The EC map of the semiconductor SWNT was acquired at a much higher driving potential (V_{appl} = −0.65 V) than the metallic nanotube (V_{appl} = −0.35 V) to detect a response. Scan profiles, forward (red) and reverse (black) for each SWNT (marked with a white dashed line on the corresponding map) are shown. (b) Linear sweep voltammograms (starting potential V_{appl} = −0.15 V) obtained using SECCM setup in static mode with the meniscus centered over an individual SWNT (black line for metallic, left-hand *y*-axis; red line for semiconductor SWNT, right-hand *y*-axis) at 50 mV s^{-1}. All potentials are given with respect to Ag/AgCl, 25 mM KCl.

tacts[23,24] results in an ohmic drop that would impact signficiantly on macroscopic SWNT-based electrochemical measurements and devices, especially because statistically two-thirds of the SWNT in an ensemble are semiconducting.[24] However, the very low electrochemical currents inherent to SECCM make it almost immune to such ohmic drop effects. Thus, the major difference in the response of the two SWNTs for $Ru(NH_3)_6^{3+}$ shown in Figure 4, evident in the redox-activity maps (Figure 4a) and cyclic voltammetry recorded with a static SECCM probe centered over the SWNTs (Figure 4b), can be attributed to the redox potential of the $Ru(NH_3)_6^{3+/2+}$ couple lying in the charge depletion region of semiconducting SWNTs.[30] The metallic SWNT exhibits high and uniform activity, yielding a k_0 value of 10 ± 5 cm s^{-1}, of the same order as previous work on CNT networks[7] and comparable to metal nanoelectrodes.[28] On the semiconducting SWNT, electrochemical currents were only measurable at high driving potentials with a peak current (meniscus centered over the SWNT) of just 50 fA (see line profile in Figure 4a for an electrode potential of V_{appl} = −0.65 V). At this potential, in addition to $Ru(NH_3)_6^{3+}$ reduction the current could have contributions from oxygen reduction. This could explain the small enhancement in current that is detectable at the kink in the semiconductor SWNT where defects would accumulate[31] and would be expected to exhibit a higher catalytic activity.[2]

To conclude, we have been able to characterize in detail the electrochemical activity of as-grown, pristine SWNTs at the nanoscale for the first time and relate the behavior directly to the structural and electronic properties of the SWNT. SECCM imaging has enabled us to demonstrate definitively that SWNT sidewalls are essentially uniformly active for outer-sphere redox processes and that SWNTs with metallic character are as electrochemically active as metal electrodes. The SECCM/SWNT configuration allows a wide range of kinetics to be accessed, together with the ability to picture EC activity. The platform described with the possibility of executing multiple independent experimental measurements should be generally versatile for electrochemical interfacial studies[12,32,33] and readily extrapolated to a wide range of electrode materials from modified SWNTs to emerging classes of one-dimensional nanoscale electrode materials, such as nanowires and nanoribbons.

dx.doi.org/10.1021/nl403752e | *Nano Lett.* XXXX, XXX, XXX−XXX

■ ASSOCIATED CONTENT

Supporting Information

Sample preparation and characterization, details of SECCM experiments and numerical simulations. This material is available free of charge via the Internet at http://pubs.acs.org.

■ AUTHOR INFORMATION

Corresponding Author

*E-mail: p.r.unwin@warwick.ac.uk.

Notes

The authors declare no competing financial interest.

■ ACKNOWLEDGMENTS

This project was supported by the European Research Council through Project ERC-2009-AdG 247143-QUANTIF and EPSRC (EP/H023909/1 and MOAC CDT studentship) with additional support from the National Physical Laboratory. Equipment used in this research was obtained through Science City (AM2), with support from Advantage West Midlands and partial funding by the European Regional Development Fund. The authors thank Anatolii Cuharuc for useful discussions and appreciate the expert contributions of K. McKelvey and A. Colburn for instrumentation development.

■ REFERENCES

(1) Simon, P.; Gogotsi, Y. *Nat. Mater.* **2008**, *7* (11), 845−854.
(2) Li, Y.; Zhou, W.; Wang, H.; Xie, L.; Liang, Y.; Wei, F.; Idrobo, J.-C.; Pennycook, S. J.; Dai, H. *Nat. Nanotechnol.* **2012**, *7* (6), 394−400.
(3) Wang, J. *Electroanalysis* **2005**, *17* (1), 7−14.
(4) Dumitrescu, I.; Unwin, P. R.; Macpherson, J. V. *Chem. Commun.* **2009**, *45* (45), 6886−6901.
(5) McCreery, R. L. *Chem. Rev.* **2008**, *108* (7), 2646−2687.
(6) Heller, I.; Kong, J.; Heering, H. A.; Williams, K. A.; Lemay, S. G.; Dekker, C. *Nano Lett.* **2005**, *5* (1), 137−142.
(7) Güell, A. G.; Ebejer, N.; Snowden, M. E.; McKelvey, K.; Macpherson, J. V.; Unwin, P. R. *Proc. Natl. Acad. Sci. U.S.A.* **2012**, *109* (29), 11487−92.
(8) Dudin, P. V.; Snowden, M. E.; Macpherson, J. V.; Unwin, P. R. *ACS Nano* **2011**, *5* (12), 10017−10025.
(9) Kim, J.; Xiong, H.; Hofmann, M.; Kong, J.; Amemiya, S. *Anal. Chem.* **2010**, *82* (5), 1605−1607.
(10) Wilder, J. W. G.; Venema, L. C.; Rinzler, A. G.; Smalley, R. E.; Dekker, C. *Nature* **1998**, *391* (6662), 59−62.
(11) Fan, Y.; Goldsmith, B. R.; Collins, P. G. *Nat. Mater.* **2005**, *4* (12), 906−911.
(12) Goldsmith, B. R.; Coroneus, J. G.; Khalap, V. R.; Kane, A. A.; Weiss, G. A.; Collins, P. G. *Science* **2007**, *315* (5808), 77−81.
(13) Heller, I.; Kong, J.; Williams, K. A.; Dekker, C.; Lemay, S. G. *J. Am. Chem. Soc.* **2006**, *128* (22), 7353−7359.
(14) Li, S.; Yu, Z.; Rutherglen, C.; Burke, P. J. *Nano Lett.* **2004**, *4* (10), 2003−2007.
(15) Javey, A.; Guo, J.; Wang, Q.; Lundstrom, M.; Dai, H. *Nature* **2003**, *424* (6949), 654−657.
(16) Zhang, R.; Zhang, Y.; Zhang, Q.; Xie, H.; Wang, H.; Nie, J.; Wen, Q.; Wei, F. *Nat. Commun.* **2013**, *4*, 1727.
(17) Ebejer, N.; Güell, A. G.; Lai, S. C. S.; McKelvey, K.; Snowden, M. E.; Unwin, P. R. *Annu. Rev. Anal. Chem.* **2013**, *6* (1), 329−351.
(18) Ebejer, N.; Schnippering, M.; Colburn, A. W.; Edwards, M. A.; Unwin, P. R. *Anal. Chem.* **2010**, *82* (22), 9141−9145.
(19) Güell, A. G.; Ebejer, N.; Snowden, M. E.; Macpherson, J. V.; Unwin, P. R. *J. Am. Chem. Soc.* **2012**, *134* (17), 7258−7261.
(20) Lai, S. C. S.; Dudin, P. V.; Macpherson, J. V.; Unwin, P. R. *J. Am. Chem. Soc.* **2011**, *133* (28), 10744−10747.
(21) Snowden, M. E.; Güell, A. G.; Lai, S. C. S.; McKelvey, K.; Ebejer, N.; O'Connell, M. A.; Colburn, A. W.; Unwin, P. R. *Anal. Chem.* **2012**, *84* (5), 2483−2491.
(22) Aaronson, B. D. B.; Chen, C.-H.; Li, H.; Koper, M. T. M.; Lai, S. C. S.; Unwin, P. R. *J. Am. Chem. Soc.* **2013**, *135* (10), 3873−3880.
(23) Manohara, H. M.; Wong, E. W.; Schlecht, E.; Hunt, B. D.; Siegel, P. H. *Nano Lett.* **2005**, *5* (7), 1469−1474.
(24) Biercuk, M.; Ilani, S.; Marcus, C.; McEuen, P., Electrical Transport in Single-Wall Carbon Nanotubes. In *Carbon Nanotubes*; Springer: Berlin, 2008; Vol. *111*, pp 455−493.
(25) Frank, S.; Poncharal, P.; Wang, Z. L.; Heer, W. A. d. *Science* **1998**, *280* (5370), 1744−1746.
(26) Bard, A. J.; Faulkner, L. R. *Electrochemical Methods - Fundamentals and Applications*, 2nd ed.; John Wiley & Sons, Inc.: New York, 2001.
(27) Horrocks, B. R.; Mirkin, M. V.; Bard, A. J. *J. Phys. Chem.* **1994**, *98* (37), 9106−9114.
(28) Sun, P.; Mirkin, M. V. *Anal. Chem.* **2006**, *78* (18), 6526−6534.
(29) Watkins, J. J.; Chen, J.; White, H. S.; Abruña, H. D.; Maisonhaute, E.; Amatore, C. *Anal. Chem.* **2003**, *75* (16), 3962−3971.
(30) Day, T. M.; Wilson, N. R.; Macpherson, J. V. *J. Am. Chem. Soc.* **2004**, *126* (51), 16724−16725.
(31) Suenaga, K.; Wakabayashi, H.; Koshino, M.; Sato, Y.; Urita, K.; Iijima, S. *Nat. Nanotechnol.* **2007**, *2* (6), 358−360.
(32) Rosenblatt, S.; Yaish, Y.; Park, J.; Gore, J.; Sazonova, V.; McEuen, P. L. *Nano Lett.* **2002**, *2* (8), 869−872.
(33) Xia, J.; Chen, F.; Li, J.; Tao, N. *Nat. Nanotechnol.* **2009**, *4* (8), 505−509.